

Dissipative chaos and steady state of open Tavis-Cummings dimer

Debabrata Mondal¹, Andrey Kolovsky^{2,3}, S. Sinha¹

¹Indian Institute of Science Education and Research-Kolkata, Mohanpur, Nadia-741246, India

²Kirensky Institute of Physics, Federal Research Centre KSC SB RAS, 660036 Krasnoyarsk, Russia

³School of Engineering Physics and Radio Electronics, Siberian Federal University, 660041 Krasnoyarsk, Russia

We consider a coupled atom-photon system described by the Tavis-Cummings dimer (two coupled cavities) in the presence of photon loss and atomic pumping, to investigate the quantum signature of dissipative chaos. The appropriate classical limit of the model allows us to obtain a phase diagram identifying different dynamical phases, especially the onset of chaos. Both classically and quantum mechanically, we demonstrate the emergence of a steady state in the chaotic regime and analyze its properties. The interplay between quantum fluctuation and chaos leads to enhanced mixing dynamics and dephasing, resulting in the formation of an incoherent photonic fluid. The steady state exhibits an intriguing phenomenon of subsystem thermalization even outside the chaotic regime; however, its effective temperature increases with the degree of chaos. Moreover, the statistical properties of the steady state show a close connection with the random matrix theory. Finally, we discuss the experimental relevance of our findings, which can be tested in cavity and circuit quantum electrodynamics setups.

Introduction: Understanding the signature of chaos in quantum systems [1–3] still remains a vibrant area of research over the past decade. In spite of the lack of phase-space trajectories in quantum systems, the Bohigas-Giannoni-Schmit (BGS) conjecture plays a pivotal role in diagnosing chaos from spectral statistics of the Hamiltonian system [2]. While the connection between chaos, thermalization, and ergodicity in isolated quantum systems has been investigated extensively [4–9], it is less explored in open quantum systems [10–19], particularly regarding the fate of thermal steady states in dissipative environments [17–20]. In recent years there has been an impetus to study dissipative quantum chaos from spectral properties of the Liouvillian [10, 21–25], however, such correspondence remains unclear for certain systems [25]. On the other hand, the classical-quantum correspondence in collective quantum systems with an appropriate semiclassical limit can facilitate the detection of chaos in the quantum counterpart [10–14, 26–32].

Ultracold atomic systems coupled to cavity modes offer a pathway to study open quantum systems, where dissipation naturally arises from various loss processes [33–52]. Such atom-photon systems have recently been realized experimentally in cavity and circuit quantum electrodynamics (QED) setups, exhibiting intriguing nonequilibrium phenomena [41, 53–61]. Within a certain regime, a collection of two-level atoms interacting with a single cavity mode can be described by the Tavis-Cummings model [62, 63], which also facilitates the study of classical-quantum correspondence due to the appropriate classical limit for a large number of atoms.

In this work, we explore different dynamical phases, especially the onset of chaos and its quantum signature, in a dimer of atom-photon system under dissipation, which offers classical-quantum correspondence. Our study focuses on the properties of the emergent steady state in

the chaotic regime, particularly the combined effects of quantum fluctuations and chaos on mixing dynamics and dephasing. Furthermore, we delve into the issue of thermalization in this open quantum system and examine the statistical properties of the steady-state density matrix.

Model and semiclassical analysis: We consider two coupled cavities, each containing N two-level atoms interacting with a single cavity mode, which can be described by the Tavis-Cummings dimer (TCD) model with the following Hamiltonian

$$\hat{\mathcal{H}} = -J \left(\hat{a}_L^\dagger \hat{a}_R + \hat{a}_R^\dagger \hat{a}_L \right) + \sum_{i=L,R} \left[\omega \hat{a}_i^\dagger \hat{a}_i + \omega_0 \hat{S}_{zi} + \frac{\lambda}{\sqrt{2S}} \left(\hat{a}_i^\dagger \hat{S}_i^- + \hat{a}_i \hat{S}_i^+ \right) \right], \quad (1)$$

where the site index $i = L(R)$ represents left(right) cavity, \hat{a}_i annihilates photon mode with frequency ω , and J is the hopping amplitude of the photons between the cavities. Collectively, N two-level atoms with energy gap ω_0 can be represented by large spins \hat{S}_i with magnitude $S = N/2$, and λ is the atom-photon coupling strength. Note that the total excitation $\hat{\mathcal{N}} = \sum_i (\hat{a}_i^\dagger \hat{a}_i + S + \hat{S}_{zi})$ is conserved as a result of U(1) symmetry of $\hat{\mathcal{H}}$ [63]. The integrability of the single-cavity Tavis-Cummings model is broken by coupling two such cavities.

Photon loss from cavities can be compensated by atomic pumping, leading to the non-unitary evolution of the density matrix (DM) $\hat{\rho}$ described by the Lindblad master equation [64–66],

$$\dot{\hat{\rho}} = -i[\hat{\mathcal{H}}, \hat{\rho}] + \kappa \sum_i \mathcal{D}[\hat{a}_i] + \frac{1}{S} \sum_i (\gamma_\uparrow \mathcal{D}[\hat{S}_i^+] + \gamma_\downarrow \mathcal{D}[\hat{S}_i^-]), \quad (2)$$

with $\mathcal{D}[\hat{L}] = \frac{1}{2} \left(2\hat{L}\hat{\rho}\hat{L}^\dagger - \hat{L}^\dagger\hat{L}\hat{\rho} - \hat{\rho}\hat{L}^\dagger\hat{L} \right)$ describing the dissipative process corresponding to the Lindblad operator \hat{L} . The dissipators $\hat{L} = \hat{a}_i$ and \hat{S}_i^- account for the decay processes of photon and spins with amplitudes κ and

γ_\downarrow respectively. The incoherent pumping of the atoms is represented by $\mathcal{D}[\hat{S}_i^+]$ with rate $\gamma_\uparrow > \gamma_\downarrow$. From the time evolved DM, we obtain an average of any operator \hat{O} using $\langle \hat{O} \rangle = \text{Tr}(\hat{\rho}\hat{O})$. Note that, in the presence of dissipation, total excitation number $\hat{\mathcal{N}}$ is no longer conserved. Throughout the paper, we set $\hbar, k_B = 1$ and scale energy (time) by $J(1/J)$.

For $S \gg 1$, the scaled operators $\hat{\alpha}_i = (\hat{x}_i + i\hat{p}_i)/\sqrt{2} = \hat{\alpha}_i/\sqrt{S}$ and $\hat{s}_i = \hat{S}_i/S$ attain classical limit, as they satisfy, $[\hat{\alpha}_i, \hat{\alpha}_i^\dagger] = 1/S$ and $[\hat{s}_{ai}, \hat{s}_{bi}] = i\epsilon_{abc}\hat{s}_{ci}/S$, where $1/S$ plays the role of reduced Planck constant. Within the mean-field approximation, the expectation of the product of operators can be decomposed as $\langle \hat{A}\hat{B} \rangle = \langle \hat{A} \rangle \langle \hat{B} \rangle$, which is valid for $S \rightarrow \infty$ [32, 52, 67]. The semiclassical dynamics of the scaled observables is obtained from Eq.(2), which is described by the following equations of motion (EOM),

$$\dot{\alpha}_i = -(\kappa/2 + i\omega)\alpha_i - \frac{i}{\sqrt{2}}\lambda s_i^- + i\alpha_j \quad (3a)$$

$$\dot{s}_i^+ = i\omega_0 s_i^+ - i\lambda\sqrt{2}s_{zi}\alpha_i^* - f_c s_{zi}s_i^+ \quad (3b)$$

$$\dot{s}_{zi} = -\frac{i}{\sqrt{2}}\lambda(\alpha_i s_i^+ - \alpha_i^* s_i^-) + f_c(1 - s_{zi}^2) \quad (3c)$$

where $j \neq i$, $f_c = \gamma_\uparrow - \gamma_\downarrow$, $\alpha_i = \sqrt{n_i} \exp(-i\psi_i) = (x_i + ip_i)/\sqrt{2}$ and $\vec{s}_i = (\sin\theta_i \cos\phi_i, \sin\theta_i \sin\phi_i, \cos\theta_i)$.

Next, we investigate the stable fixed points (FP) and other attractors of the EOM (see Eq.(3)), describing various nonequilibrium phases of this open TCD, listed below and summarized in the phase diagram in Fig.1(a).

Normal phase (NP): This phase is characterized by vanishing photon number $n_i^* = 0$ and spin polarization $s_{zi}^* = 1$.

Superradiant phase (SR): At a critical coupling λ_c the normal phase undergoes a continuous transition to the superradiant phase (see Fig.1(a)) with a non-vanishing photon number $n^* \neq 0$ and spin polarization $|s_z^*| < 1$, same for each cavity. Due to the $U(1)$ symmetry, FPs lie on a circle of radius $\sqrt{2n^*}$ ($\sqrt{1 - (s_z^*)^2}$) in $x-p$ ($s_x - s_y$) plane, where the dynamics always converges regardless of the initial condition. The details of this phase are given in the supplementary material [68].

Oscillatory phase (OP): Once the SR phase becomes unstable for $\lambda > \lambda_I$ (see Fig.1(a,c,d)), the oscillatory phase emerges, where the periodic motion is identified from a single peak in the Fourier transform of trajectories [68]. Although the photon number oscillates, its phase in both cavities remains the same $\psi_L = \psi_R$, similar to the SR phase.

Coexistence of chaos and oscillatory dynamics: Further increasing λ gives rise to the mixed type of dynamics, where oscillatory motion coexists with chaotic dynamics, depending on the initial conditions.

Chaotic dynamics: We also identify a regime in the phase diagram where the trajectories exhibit chaotic behavior, as depicted in Fig.1(b). To quantify the degree

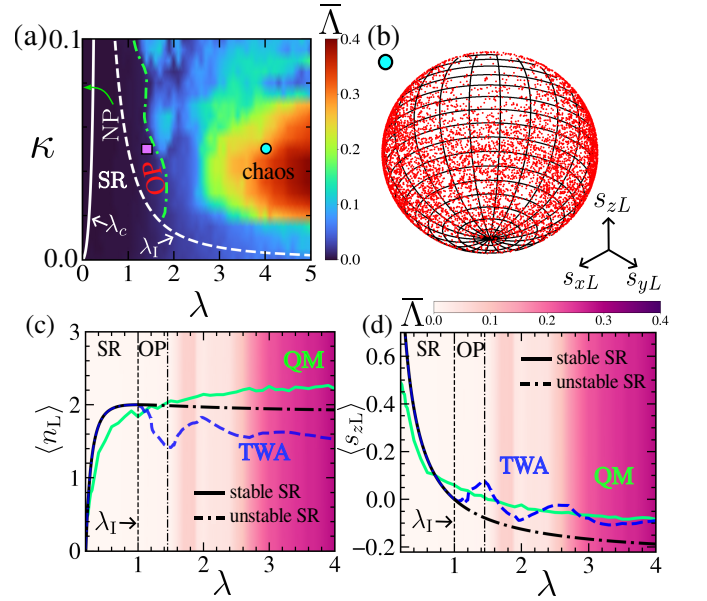


FIG. 1. *Dynamical phases and steady states:* (a) The classical phase-diagram in λ - κ plane with average Lyapunov exponent $\bar{\Lambda}$ as color scale. The NP to SR transition at λ_c (solid line) and instability of SR phase at λ_I (dashed line) are shown. (b) The chaotic trajectory is represented by scattered points on the Bloch sphere at regular time intervals ($\lambda = 4.0, \kappa = 0.05$ (blue circle in (a))). *Steady state:* Variation of average (c) photon number $\langle n_L \rangle$ and (d) spin polarization $\langle s_{zL} \rangle$ of one cavity with λ for $\kappa = 0.05$. TWA results (blue dashed line), quantum steady-state value (solid green line) and fixed point (n^*, s_z^*) of SR phase are compared. The stable (unstable) SR phase is shown by black solid (dashed dotted) line. The color scales in (c,d) represent $\bar{\Lambda}$. All energies (time) are measured by $J(1/J)$. We set $\hbar, k_B = 1$ and $\omega = 2.0, \omega_0 = 0.5, \gamma_\uparrow = 0.2, \gamma_\downarrow = 0.1, S = 2$ for all figures.

of chaos, we compute the mean Lyapunov exponent $\bar{\Lambda}$ [69–71] averaged over random initial phase space points, as shown in Fig.1(a).

The stable fixed point attractors, such as NP and SR phases, uniquely describe the system's asymptotic steady state. To understand the state of the system after the instability of the SR phase, we study the semiclassical dynamics on an ensemble of phase space points using truncated Wigner approximation (TWA) [72–74]. Quantum fluctuations are incorporated by sampling initial conditions from the Husimi distribution [75] of a product of bosonic and spin coherent states, $|\Psi_c\rangle = \prod_i |\alpha_i\rangle \otimes |s_{zi}, \phi_i\rangle$ [76] corresponding to large spin $S \gg 1$, which semiclassically represents an arbitrary phase space point $\{\alpha_i, s_{zi} = \cos\theta_i, \phi_i\}$. Importantly, we observe the emergence of a unique steady state in both oscillatory and chaotic phases, characterized by the stationary value of physical quantities such as photon number $\langle n \rangle_{\text{TWA}}$ and spin polarization $\langle s_z \rangle_{\text{TWA}}$ after sufficient time, which smoothly connects to the stable SR phase, as shown in Fig.1(c,d). Moreover, these dynamical variables follow stationary

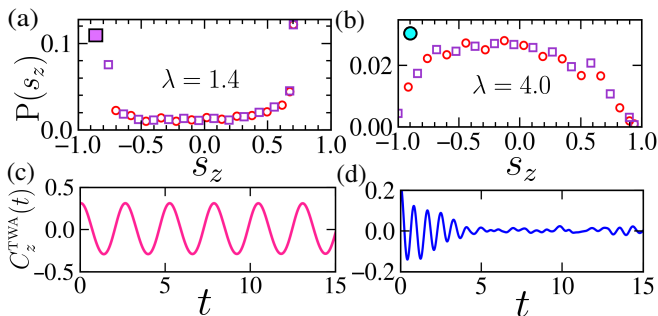


FIG. 2. *Comparison between oscillatory and chaotic phases:* Steady-state distribution and autocorrelation function of the spin polarization s_z of one of the cavities in the (a,c) oscillatory (OP) ($\lambda = 1.4$, violet square in Fig.1(a)), (b,d) chaotic regime ($\lambda = 4.0$, blue circle in Fig.1(a)). Squares and circles in (a,b) represent distributions starting from different initial conditions. We choose $\kappa = 0.05$.

distribution $P(n_i)$, $P(s_{zi})$ irrespective of initial condition (see Fig.2(a,b)). Notably, Our analysis reveals the ergodic nature of the steady state, which is based on (i) the equivalence between time and ensemble averages $\langle O \rangle_t = \langle O \rangle_{\text{TWA}}$ of dynamical quantities and (ii) their independence from initial condition [77–80].

The different dynamical regimes of the steady state particularly, the onset of chaos can be revealed from the autocorrelation function,

$$C^{TWA}(t) = \langle O(t+\tau)O(\tau) \rangle - \langle O(t+\tau) \rangle \langle O(\tau) \rangle, \quad (4)$$

computed within TWA. Here, the observable O is first evolved up to a long transient time τ until $\langle O(\tau) \rangle_{\text{TWA}}$ reaches the steady state. Although the TWA analysis indicates the formation of a steady state in the oscillatory regime, the autocorrelation function exhibits persistent oscillations, revealing its signature (see Fig.2(c)). On the contrary, in the chaotic regime, the autocorrelation function decays rapidly, as seen from Fig.2(d), confirming chaotic mixing [79–81]. Interestingly, the steady state in the oscillatory regime displays ergodicity in the absence of mixing. This contrasts with the typical closed system, where chaotic mixing leads to the ergodic steady state.

Quantum steady state: To this end, we investigate the properties of the quantum steady state and the signature of chaos in the presence of quantum fluctuation. We obtain the steady state density matrix (DM) $\hat{\rho}_{\text{ss}}$ by solving the Master equation (see Eq.(2)) using the stochastic wavefunction approach [75, 82, 83], considering spin magnitude $S = 2$. Similar to the classical analysis, a unique quantum steady state is formed across different dynamical regimes with increasing coupling strength. This state is characterized by the average quantities $\langle \hat{n}_i \rangle_{\text{ss}}$ and $\langle \hat{S}_{zi} \rangle_{\text{ss}}$ obtained from $\hat{\rho}_{\text{ss}}$, as shown in Fig.1(c,d). For comparison with classical results, we scale these physical quantities by S . The steady state also exhibits ergodicity analogous to its classical counterpart, as the time

average of the observables $\langle \hat{n}_i \rangle_t$ and $\langle \hat{S}_{zi} \rangle_t$ over a typical quantum trajectory approach to their steady-state values $\langle \hat{n}_i \rangle_{\text{ss}}$ and $\langle \hat{S}_{zi} \rangle_{\text{ss}}$ respectively [68].

Next, we study the nonequilibrium dynamics to investigate the signature of quantum mixing, as the chaotic regime is approached with increasing λ . Starting from an arbitrary initial coherent state $|\Psi_c\rangle$, representing a phase space point, we study the time evolution of survival probability $f(t) = \text{Tr}(\hat{\rho}(t)\hat{\rho}(0))$ [84–87] between the initial and time-evolved density matrices. The survival probability $f(t)$, averaged over an ensemble of initial states, decays exponentially with time and the decay rate increases as we approach the chaotic regime (see Fig.3(b)).

From the time evolved density matrix, we also obtain the total entropy $\mathcal{S}_{\text{tot}} = -\text{Tr}(\hat{\rho}(t) \ln \hat{\rho}(t))$, which grows linearly and attains a saturation value corresponding to the steady state. As evident from Fig.3(a), both the growth rate and the saturation value of \mathcal{S}_{tot} increases with λ . Also, the reduced density matrix $\hat{\rho}_A = \text{Tr}_{\bar{A}}(\hat{\rho})$ of subsystem A can be obtained by tracing out the remaining degrees of freedom \bar{A} , which in turn yields the corresponding entanglement entropy (EE) $\mathcal{S}_A = -\text{Tr}(\hat{\rho}_A \ln \hat{\rho}_A)$. Additionally, the EE corresponding to one of the cavities \mathcal{S}_L exhibits similar behavior [68]. Such linear growth in EE is typically observed as a signature of chaos in isolated quantum systems [4, 6, 88–91]. The underlying chaos can also be unveiled from the individual quantum trajectories, which show a spreading of the power spectrum over a wide range of frequencies

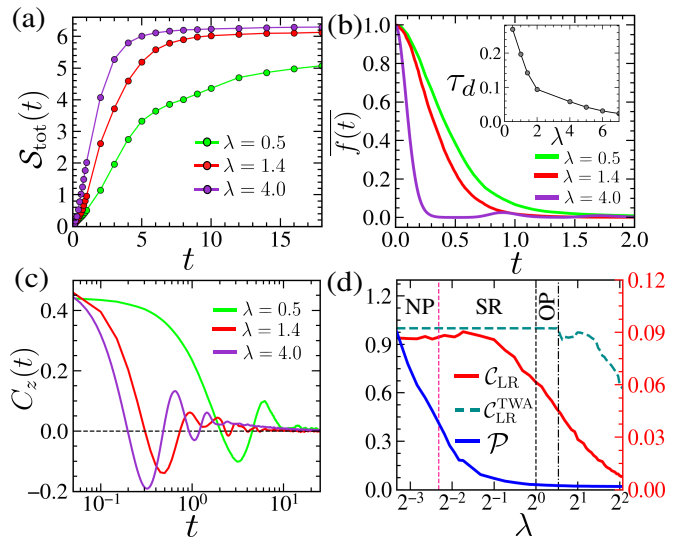


FIG. 3. *Quantum dynamics:* (a) Evolution of total entropy \mathcal{S}_{tot} and (b) survival probability $f(t)$ at different coupling λ . Inset in (b) shows variation of decay time τ_d of $f(t)$ with λ . (c) Dynamics of autocorrelation of spin $C_z(t)$ for different λ . (d) Steady-state value of the coherence function C_{LR} of the photon field between the cavities (solid red), corresponding TWA result (dashed greenish blue) and the purity \mathcal{P} (solid blue, right axis), as a function of λ . For all figures, $\kappa = 0.05$.

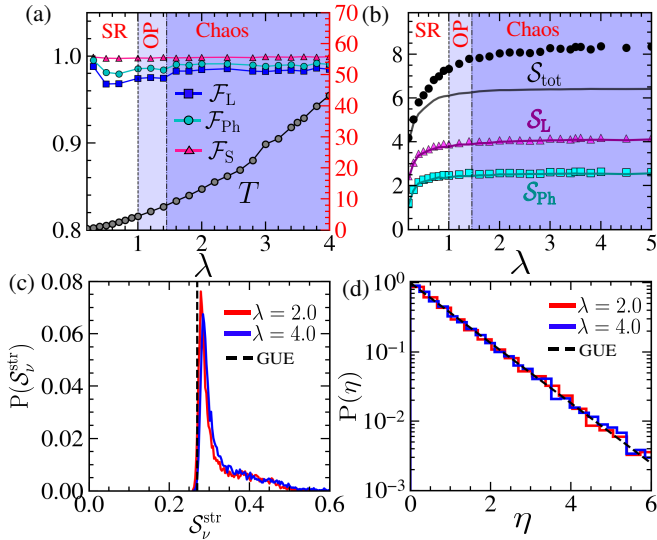


FIG. 4. *Subsystem thermalization*: (a) Overlap between subsystem reduced DM obtained from the steady state $\hat{\rho}_{ss}$ and the corresponding DM derived from the thermal state $\hat{\rho}^{th}$. The overlap of the left cavity (\mathcal{F}_L), photon (\mathcal{F}_{Ph}), spin (\mathcal{F}_S) of the same cavity (left axis) and effective temperature T (right axis) as a function of λ . Variation of (b) total entropy \mathcal{S}_{tot} , entanglement entropy of the left cavity \mathcal{S}_L and photon field of that cavity \mathcal{S}_{Ph} in the steady state $\hat{\rho}_{ss}$ with λ . The solid lines (markers) represent the entropies obtained from $\hat{\rho}_{ss}$ ($\hat{\rho}^{th}$). Classical phases are marked by blue colored regimes. *Statistics of $\hat{\rho}_{ss}$* : (c) distribution of structural entropy \mathcal{S}_ν^{str} of eigenstates of $\hat{\rho}_{ss}$ in the chaotic regime. Black dashed line represents the corresponding GUE value. (d) Distribution of elements $\eta = |\Psi_\nu^j|^2 N_{dim}$ of typical eigenstate of steady state at different λ . Black dashed line represents the corresponding GUE distribution. Parameter chosen: $\kappa = 0.05$.

[68, 92].

We also analyze the autocorrelation function corresponding to the steady state $C(t) = \langle O(t)O(0) \rangle - \langle O(t) \rangle \langle O(0) \rangle$, following the prescription of stochastic wave-function [83, 93]. As seen from Fig.3(c), the autocorrelation function $C_z(t)$ of the spin in one cavity vanishes rapidly and the decay time decreases with increasing coupling strength λ . Such fast decay of $C_z(t)$ signifies enhanced mixing dynamics due to the onset of chaos.

In addition, the quantum fluctuations enhance the decay rate of $C_z(t)$ as compared to the classical counterpart. Importantly, the oscillatory phase is washed out due to the strong quantum fluctuation, which is evident from the decaying autocorrelation function (see Fig.3(c)). Furthermore, the combined effect of quantum fluctuations and chaotic mixing suppresses the purity of the steady state $\mathcal{P} = \text{Tr}(\hat{\rho}_{ss}^2)$ significantly, even in the superradiant phase, as depicted in Fig.3(d). The coherence of the photon fields between the two cavities in the steady state can

be quantified from,

$$\mathcal{C}_{LR} = \frac{\langle \hat{a}_L^\dagger \hat{a}_R + \hat{a}_R^\dagger \hat{a}_L \rangle}{2\sqrt{\langle \hat{n}_L \rangle \langle \hat{n}_R \rangle}}, \quad (5)$$

which classically reduces to $\mathcal{C}_{LR}^{TWA} = \langle \cos(\psi_L - \psi_R) \rangle_{TWA}$. In the superradiant and oscillatory phase, \mathcal{C}_{LR}^{TWA} attains the value unity and decays in the chaotic regime, as observed from the TWA analysis. Similar behavior can also be observed quantum mechanically, however, the decay starts even before the instability of SR phase, as a result of quantum fluctuations (see Fig.3(d)). It is clear from this analysis that the mixing dynamics due to the underlying chaos as well as quantum fluctuation can lead to the destruction of the coherence of the system, which can be probed from the state of the photon field of the respective cavities. The semiclassical distribution of the photon field for the sufficiently small value of λ in the stable SR phase is peaked around the circle of the classical fixed points of radius $\sqrt{2n^*}$. As we approach the chaotic regime, this distribution spreads and peaks around the center, resembling a thermal distribution [68]. Such an observation suggests chaos-induced thermalization in this dissipative system, which we discuss next.

Subsystem thermalization: To investigate thermalization of this open system, we consider the thermal density matrix of TCD $\hat{\rho}^{th} = \exp(-\beta(\hat{\mathcal{H}} - \mu\hat{\mathcal{N}}))/Z$ with Z being the partition function. The inverse temperature β and the chemical potential μ are uniquely determined from the mean energy $\langle \hat{\mathcal{H}} \rangle$ and the average number of excitations $\langle \hat{\mathcal{N}} \rangle$ obtained from the steady-state density matrix $\hat{\rho}_{ss}$. Clearly, $\hat{\rho}^{th}$ does not correspond to the steady state of the Master equation (Eq.(2)) in the presence of dissipation. However, the state of the subsystem A can be well described by the reduced DM $\hat{\rho}_A^{th}$ derived from the thermal state $\hat{\rho}^{th}$ of the full system. We compare the reduced DMs $\hat{\rho}_A^{ss}$ and $\hat{\rho}_A^{th}$ obtained from the steady state and thermal DM respectively, using their overlap $\mathcal{F}_A = \text{Tr} \sqrt{\sqrt{\hat{\rho}_A^{ss}} \hat{\rho}_A^{th} \sqrt{\hat{\rho}_A^{ss}}}$ [84, 85]. Considering one of the cavities as well as its photonic and spin sector as subsystems, we compute \mathcal{F}_A , which remains close to unity, as evident from Fig.4(a). Moreover, trace-distances between $\hat{\rho}_A^{ss}$ and $\hat{\rho}_A^{th}$ remain small [68], indicating the similarity between them. Consequently, the entanglement entropies of the corresponding subsystems (see Fig.4(b)) as well as the average values of the observables such as $\langle \hat{n}_i \rangle$ and $\langle \hat{S}_{zi} \rangle$ exhibit agreement with those of the thermal state [68], confirming the validity of subsystem thermalization [94–96] in open TCD over a range of λ . Surprisingly, the steady state follows the subsystem thermalization over a large range of coupling strength even outside the chaotic regime, however, the effective temperature T increases with the degree of chaos, as shown in Fig.4(a). For a deeper understanding of this scenario, we also study the statistics of eigenstates $|\Psi_\nu\rangle$ of the steady-state DM $\hat{\rho}_{ss}$. We compute the structural entropy [97, 98] of

$|\Psi_\nu\rangle$,

$$\mathcal{S}_\nu^{\text{str}} = - \sum_j |\Psi_\nu^j|^2 \ln(|\Psi_\nu^j|^2) + \ln \left(\sum_j |\Psi_\nu^j|^4 \right), \quad (6)$$

and study its distribution, which is sharply peaked around a value $\mathcal{S}^{\text{str}} \approx 0.27$ (see Fig.4(c)) corresponding to the Gaussian unitary ensemble (GUE) class of the random matrix theory (RMT) [3, 99]. Moreover, the elements $\eta = |\Psi_\nu^j|^2 N_{\text{dim}}$ of the eigenstate $|\Psi_\nu\rangle$ (with dimension N_{dim}), follows the GUE distribution $P(\eta) = \exp(-\eta)$ [1], as seen from Fig.4(d), indicating the chaotic nature of such states. The steady state of a random Liouvillian also follows the GUE distribution [22, 100], however in the present case, we do not find any signature of level repulsion in the Liouvillian spectrum, which on the contrary resembles to 2d-Poisson distribution, even in the chaotic regime [68].

Discussion: Our study unveils the emergence of a steady state with intriguing properties, especially the onset of chaos in an open atom-photon dimer system. The appropriate classical limit of this system enables us to explore the classical-quantum correspondence of dissipative chaos, which is absent in a generic quantum system. The rapid decay of the correlation function and survival probability, along with the growth of entropy, manifest the chaotic mixing of the emergent steady state, which serves as a more tangible signature of dissipative chaos compared to spectral statistics. Both chaos and quantum fluctuations result in the loss of coherence, leading to the formation of an incoherent photonic fluid, which can be probed experimentally. Remarkably, this steady state follows thermalization of the subsystems, revealing its connection with the random matrix.

In conclusion, this atom-photon dimer system exhibits intriguing nonequilibrium phenomena and sheds light on dissipative quantum chaos, with results readily testable in current cavity and circuit QED setups.

Acknowledgments: We thank Krishnendu Sengupta and Sudip Sinha for comments and fruitful discussions. D.M. acknowledges support from Prime Minister Research Fellowship (PMRF).

[1] F. Haake, *Quantum Signatures of Chaos*, Springer Science and Business Media (Springer, Berlin, Heidelberg, 2013), Vol. 54.
 [2] O. Bohigas, M. J. Giannoni, and C. Schmit, Phys. Rev. Lett. **52**, 1 (1984).
 [3] F. M. Izrailev, Phys. Rep. **196**, 299 (1990);
 [4] L. D'Alessio, Y. Kafri, A. Polkovnikov, and M. Rigol, Adv. Phys. **65**, 239 (2016).
 [5] M. Ueda, Nat. Rev. Phys. **2**, 669 (2020).
 [6] F. Borgonovi, F. M. Izrailev, L. F. Santos, and V. G. Zelevinsky, Phys. Rep. **626**, 1 (2016).

[7] M. Rigol, V. Dunjko, M. Olshanii, Nature **452**, 854 (2008).
 [8] J. M. Deutsch, Phys. Rev. A **43**, 2046 (1991).
 [9] M. Srednicki, Phys. Rev. E **50**, 888 (1994).
 [10] R. Grobe, F. Haake, and Hans-Jürgen Sommers, Phys. Rev. Lett. **61**, 1899 (1988); R. Grobe and F. Haake, Phys. Rev. Lett. **62**, 2893–2896 (1989).
 [11] G. G. Carlo, G. Benenti, and D. L. Shepelyansky, Phys. Rev. Lett. **95**, 164101 (2005).
 [12] G. G. Carlo, G. Benenti, G. Casati, and D. L. Shepelyansky, Phys. Rev. Lett. **94**, 164101 (2005).
 [13] D. Dahan, G. Arwas, and E. Grosfeld, npj Quantum Inf **8**, 14 (2022).
 [14] D. Mondal, K. Sengupta, S. Sinha, [arXiv:2310.12779](https://arxiv.org/abs/2310.12779) (2023).
 [15] G. Vivek, D. Mondal, S. Chakraborty, S. Sinha, [arXiv:2405.13809](https://arxiv.org/abs/2405.13809) (2024).
 [16] F. Ferrari, L. Gravina, D. Eeltink, P. Scarlino, V. Savona, F. Minganti, [arXiv:2305.15479](https://arxiv.org/abs/2305.15479) (2023).
 [17] M. Žnidarič, T. Prosen, G. Benenti, G. Casati, and D. Rossini, Phys. Rev. E **81**, 051135 (2010).
 [18] I. Reichental, A. Klemmner, Y. Kafri, and D. Podolsky, Phys. Rev. B **97**, 134301 (2018).
 [19] T. Shirai and T. Mori, Phys. Rev. E **101**, 042116 (2020).
 [20] F. Vicentini, A. Biella, N. Regnault, and C. Ciuti, Phys. Rev. Lett. **122**, 250503 (2019).
 [21] L. Sá, P. Ribeiro, and T. Prosen, Phys. Rev. X **10**, 021019 (2020).
 [22] L. Sá, P. Ribeiro, and T. Prosen, J. Phys. A: Math. Theor. **53** 305303 (2020).
 [23] S. Denisov, T. Lapyeva, W. Tarnowski, D. Chruściński, and K. Życzkowski, Phys. Rev. Lett. **123**, 140403 (2019).
 [24] M. Prasad, H. K. Yadalam, C. Aron, and M. Kulkarni, Phys. Rev. A **105**, L050201 (2022).
 [25] D. Villaseñor, L. F. Santos, P. Barberis-Blostein, [arXiv:2406.07616](https://arxiv.org/abs/2406.07616) (2024).
 [26] C. Emary and T. Brandes, Phys. Rev. Lett. **90**, 044101 (2003);
 [27] A. Altland and F. Haake, Phys. Rev. Lett. **108**, 073601 (2012); New J. Phys. **14**, 073011 (2012).
 [28] D. Villaseñor, S. Pilatowsky-Cameo, M. A. Bastarrachea-Magnani, S. Lerma-Hernández, L. F. Santos, and J. G. Hirsch, Entropy **25**, 8 (2022).
 [29] T. Dittrich, R. Graham, Europhys. Lett. **7**, 287 (1988).
 [30] P.S.Muraev, D.N.Maksimov, and A.R.Kolovsky, Entropy **2023**, 25, 117.
 [31] A. R. Kolovsky, Phys. Rev. E **106**, 014209 (2022).
 [32] S. Sinha, S. Ray and S. Sinha, J. Phys.: Condens. Matter **36** 163001 (2024).
 [33] F. Mivehvar, F. Piazza, T. Donner, H. Ritsch, Adv. Phys. **70**, 1–153 (2021).
 [34] H. Ritsch, P. Domokos, F. Brennecke, and T. Esslinger, Rev. Mod. Phys. **85**, 553 (2013).
 [35] M. Müller, S. Diehl, G. Pupillo, and P. Zoller, Adv. At. Mol. Opt. Phys. **61**, 1 (2012).
 [36] F. Damanet, E. Mascarenhas, D. Pekker, and A. J. Daley, Phys. Rev. Lett. **123**, 180402 (2019).
 [37] P.M. Harrington, E.J. Mueller, and K.W. Murch, Nat Rev Phys **4**, 660–671 (2022).
 [38] R. Lin, R. Rosa-Medina, F. Ferri, F. Finger, K. Kroeger, T. Donner, T. Esslinger, and R. Chitra, Phys. Rev. Lett. **128**, 153601 (2022).

- [39] H. Weimer, A. Kshetrimayum, and R. Orús, *Rev. Mod. Phys.* **93**, 015008 (2021).
- [40] F. Damanet, A. J. Daley, and J. Keeling, *Phys. Rev. A* **99**, 033845 (2019).
- [41] J. Klinder, H. Keßler, M. Wolke, L. Mathey, and A. Hemmerich, *Proc. Natl. Acad. Sci. U.S.A.* **112**, 3290 (2015).
- [42] S. Diehl, A. Tomadin, A. Micheli, R. Fazio, and P. Zoller, *Phys. Rev. Lett.* **105**, 015702 (2010).
- [43] H. J. Carmichael, *Phys. Rev. X* **5**, 031028 (2015).
- [44] K. C. Stitely, A. Giraldo, B. Krauskopf, and S. Parkins, *Phys. Rev. Research* **2**, 033131 (2020).
- [45] K. C. Stitely, A. Giraldo, B. Krauskopf, and S. Parkins, *Phys. Rev. Research* **4**, 023101 (2022).
- [46] K. C. Stitely, S. J. Masson, A. Giraldo, B. Krauskopf, and S. Parkins, *Phys. Rev. A* **102**, 063702 (2020).
- [47] C. J. Zhu, L. L. Ping, Y. P. Yang, and G. S. Agarwal, *Phys. Rev. Lett.* **124**, 073602 (2020).
- [48] S. Ray, A. Vardi, and D. Cohen, *Phys. Rev. Lett.* **128**, 130604 (2022).
- [49] K. C. Stitely, F. Finger, R. Rosa-Medina, F. Ferri, T. Donner, T. Esslinger, S. Parkins, and B. Krauskopf, *Phys. Rev. Lett.* **131**, 143604 (2023).
- [50] J. Li, R. Fazio, and S. Chesi, *New J. Phys.* **24**, 083039 (2022).
- [51] W. Kopylov, M. Radonjić, T. Brandes, A. Balazš, and A. Pelster, *Phys. Rev. A* **92**, 063832 (2015).
- [52] F. Carollo and I. Lesanovsky, *Phys. Rev. Lett.* **126**, 230601 (2021).
- [53] J. M. Raimond, M. Brune, and S. Haroche, *Rev. Mod. Phys.* **73**, 565 (2001).
- [54] A. Blais, A. L. Grimsmo, S. M. Girvin, and A. Wallraff, *Rev. Mod. Phys.* **93**, 025005 (2021).
- [55] J. Léonard, A. Morales, P. Zupancic, T. Esslinger, and T. Donner, *Nature (London)* **543**, 87 (2017).
- [56] J. Léonard, A. Morales, P. Zupancic, T. Donner, and T. Esslinger, *Science* **358**, 1415 (2017).
- [57] J.A. Muniz, D. Barberena, R.J. Lewis-Swan, D. J. Young, J. R. K. Cline, A. M. Rey, *Nature* **580**, 602–607 (2020).
- [58] D.J. Young, A. Chu, E.Y. Song, D. Barberena, D. Wellnitz, Z. Niu, V. M. Schäfer, R. J. Lewis-Swan, A. M. Rey and J. K. Thompson, *Nature* **625**, 679–684 (2024).
- [59] F. Letscher, O. Thomas, T. Niederprüm, M. Fleischhauer, and H. Ott, *Phys. Rev. X* **7**, 021020 (2017).
- [60] R. M. Kroeze, Y. Guo, V. D. Vaidya, J. Keeling, and B. L. Lev, *Phys. Rev. Lett.* **121**, 163601 (2018).
- [61] M. Fitzpatrick, N. M. Sundaesan, A. C. Y. Li, J. Koch and A. A. Houck, *Phys. Rev. X* **7**, 011016 (2017).
- [62] M. Tavis and F. W. Cummings, *Phys. Rev.* **170**, 379 (1968).
- [63] H-P Eckle, *Models of Quantum Matter: A First Course on Integrability and the Bethe Ansatz*, Chap 12, 474 (Oxford University Press, (2021)).
- [64] V. Gorini, A. Kossakowski, and E. C. G. Sudarshan, *J. Math. Phys. (N.Y.)* **17**, 821–825 (1976).
- [65] G. Lindblad, *Commun. Math. Phys.* **48**, 119–130 (1976).
- [66] H. P. Breuer and F. Petruccione, *The Theory of Open Quantum Systems* (Oxford University Press, Oxford, 2007).
- [67] L. da Silva Souza, L. F. dos Prazeres, and F. Iemini, *Phys. Rev. Lett.* **130**, 180401 (2023).
- [68] See the Supplementary material for the details of the classical dynamical phases, quantum ergodicity, subsystem thermalization and statistics of the Liouvillian spectrum in the present model.
- [69] S. H. Strogatz, *Nonlinear Dynamics and Chaos* (Westview Press, Boulder, CO, 2007).
- [70] A. J. Lichtenberg and M. A. Leiberman, *Regular and chaotic dynamics*, (Springer-Verlag, 1992).
- [71] J. Chávez-Carlos, M. A. Bastarrachea-Magnani, S. Lerma-Hernández, and J. G. Hirsch, *Phys. Rev. E* **94**, 022209 (2016).
- [72] P. B. Blakie, A. S. Bradley, M. J. Davis, R. J. Ballagh, and C. W. Gardiner, *Adv. Phys.* **57**, 363 (2008).
- [73] A. Polkovnikov, *Ann. Phys.* **325**, 1790 (2010).
- [74] J. Schachenmayer, A. Pikovsky, and A. M. Rey, *Phys. Rev. X* **5**, 011022 (2015).
- [75] C. Gardiner and P. Zoller, *Quantum Noise: A Handbook of Markovian and Non-Markovian Quantum Stochastic Methods with Applications to Quantum Optics* (Springer Science, New York, 2004).
- [76] J. M. Radcliffe, *J. Phys. A: Gen. Phys.*, **4**, 313 (1971).
- [77] I. P. Cornfield, S. V. Fomin, and Y. G. Sinai, 1982 *Ergodic Theory* (Springer) .
- [78] P. R. Halmos 2017 *Lectures on Ergodic Theory* (Dover).
- [79] R. Frigg, J. Berkovitz, and F. Kronz, The Ergodic Hierarchy, in *The Stanford Encyclopedia of Philosophy*, (Fall 2020 Edition), edited by E. N. Zalta, <https://plato.stanford.edu/archives/fall2020/entries/ergodic-hierarchy/>.
- [80] E. Ott, *Chaos in dynamical systems* (1993, Cambridge University Press).
- [81] D. Ruelle, *Chaotic evolution and strange attractors* (1989, Cambridge University Press).
- [82] H. Carmichael, *An Open Systems Approach to Quantum Optics*. Springer-Verlag (1993).
- [83] K. Mølmer, Y. Castin and J. Dalibard, *J. Opt. Soc. Am. B* **10**, 524 (1993).
- [84] M. A. Nielsen and I. L. Chuang, *Quantum Computation and Quantum Information*, (Cambridge University Press, Cambridge, England, 2000).
- [85] H. Nha and H. J. Carmichael, *Phys. Rev. A* **71**, 032336 (2005).
- [86] F. Tonielli, R. Fazio, S. Diehl, and J. Marino, *Phys. Rev. Lett.* **122**, 040604 (2019).
- [87] For unitary dynamics of initial pure state $\hat{\rho}(0) = |\Psi(0)\rangle\langle\Psi(0)|$, the quantity $f(t) = \text{Tr}(\hat{\rho}(t)\hat{\rho}(0))$ reduces to the usual definition of survival probability $f(t) = |\langle\Psi(t)|\Psi(0)\rangle|^2$. Additionally, it is related with the more general definition of overlap between two mixed density matrices (see Ref. [84, 85]).
- [88] A. Piga, M. Lewenstein, and J. Q. Quach, *Phys. Rev. E* **99** 032213 (2019).
- [89] X. Wang, S. Ghose, B. C. Sanders, and B. Hu, *Phys. Rev. E* **70** 016217 (2004).
- [90] H. Fujisaki, T. Miyadera, and A. Tanaka, *Phys. Rev. E* **67**, 066201 (2003).
- [91] S. Ray, A. Ghosh, and S. Sinha, *Phys. Rev. E* **94**, 032103 (2016).
- [92] T. Geisel, *Phys. Rev. A* **41**, 2989 (1990); Erratum *Phys. Rev. A* **42**, 7491 (1990).
- [93] S. Wolff, A. Sheikhan, C. Kollath, *SciPost Phys. Core* **3**, 010 (2020)
- [94] A. Dymarsky, N. Lashkari, and H. Liu, *Phys. Rev. E* **97**, 012140 (2018);
- [95] Z. Huang and Xiao-Kan Guo, *Phys. Rev. E* **109**, 054120

- (2024).
- [96] J. R. Garrison and T. Grover, *Phys. Rev. X* **8**, 021026 (2018).
- [97] J. Pipek and I. Varga, *Phys. Rev. A* **46**, 3148 (1992).
- [98] P. Jacquod and I. Varga, *Phys. Rev. Lett.* **89**, 134101 (2002).
- [99] S. Ray, B. Mukherjee, S. Sinha, and K. Sengupta, *Phys. Rev. A* **96**, 023607 (2017).
- [100] T. Prosen and M. Žnidarič, *Phys. Rev. Lett.* **111**, 124101 (2013).

SUPPLEMENTARY MATERIAL:
Dissipative chaos and steady state of open Tavis-Cummings dimer

CLASSICAL ANALYSIS

For the coupled atom-photon system, a phase-space point can be represented by an array $\mathbf{X} = \{\alpha_i, s_{zi} = \cos \theta_i, \phi_i\}$, where both the cavities $i = L, R$ are included. The fixed points (FP) \mathbf{X}^* representing the steady states, satisfying $\dot{\mathbf{X}} = 0$, can be obtained from the equations of motion (given in Eq.(3) of the main text). To investigate the stability of the different phases of the open Tavis-Cummings dimer (TCD), we perform the linear stability analysis. We write the dynamical variables as $\mathbf{X}(t) = \mathbf{X}^* + \delta\mathbf{X}(t)$, representing the small fluctuation $\delta\mathbf{X}(t)$ around the FP \mathbf{X}^* . The time evolution of the fluctuations can be written as $\delta\mathbf{X}(t) = \delta\mathbf{X}(0)e^{\lambda_s t}$, where λ_s are obtained from the linearized equations and the stability of a steady state is ensured by the condition $\text{Re}(\lambda_s) < 0$ [1]. Following this procedure, we have obtained the stability regimes of the various steady states in the parameter space, as given in the phase diagram (see Fig.1(a) of the main text for details).

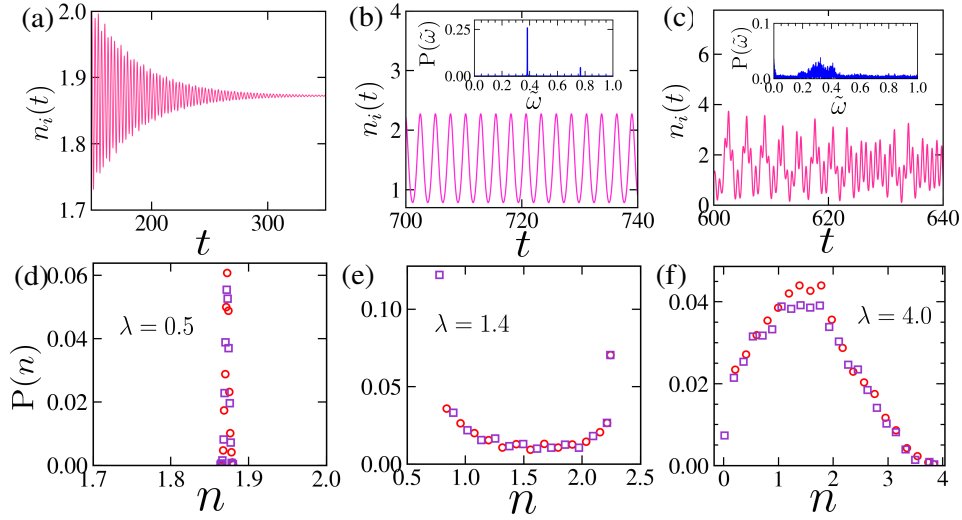


FIG. 1. *Classical dynamics*: Time evolution of the photon number $n_i(t)$ of one of the cavities in the (a) SR phase ($\lambda = 0.5$), (b) oscillatory phase ($\lambda = 1.4$) and (c) chaotic regime ($\lambda = 4.0$). The inset of (b), (c) show the Fourier spectrum of the corresponding trajectory. Distribution of the photon number n_i at long time within TWA for the (d) SR state ($\lambda = 0.5$), (e) oscillatory phase (OP) ($\lambda = 1.4$) and the (f) chaotic phase ($\lambda = 4.0$). Squares and circles in (d-f) represent distributions starting from different initial conditions. We consider $\kappa = 0.05$.

We summarize the homogenous phases ($\mathbf{X}_i = \mathbf{X}^*$) of open TCD and transitions between them. The normal phase (NP) is characterized by vanishing photon number $n^* = 0$ and spin polarization $s_z^* = 1$. The NP becomes unstable at a critical coupling λ_c and undergoes a continuous transition to superradiant phase (SR), characterized by,

$$s_z^* = -\frac{\kappa}{2f_c} + \sqrt{\frac{\kappa}{f_c} \left(\frac{\omega - \omega_0 - 1}{\sqrt{2\lambda^2 - f_c\kappa}} \right)}, \quad n^* = \frac{f_c}{\kappa} (1 - s_z^{*2}), \quad \sin(\phi^* - \psi^*) = -\frac{\sqrt{f_c\kappa}}{\lambda\sqrt{2}}, \quad (1)$$

where ϕ^* and ψ^* are phases of spin and photon field respectively. The critical coupling strength corresponding to the dissipative transition between NP and SR phases is given by,

$$\lambda_c(\kappa) = \sqrt{\frac{\kappa f_c}{2}} \sqrt{1 + \frac{4(\omega_0 - \omega + 1)^2}{(2f_c - \kappa)^2}}. \quad (2)$$

As a result of U(1) symmetry, the phase $\phi + \psi$ increases linearly in time, however, the photon number and spin polarization remain at the steady value n^*, s_z^* (see Fig.1(a)). To describe the SR phase as a steady state, it is necessary to switch into a rotating frame with the frequency Ω , where the photon field and spin projection in $x - y$ plane evolve as $\alpha_i \rightarrow \alpha_i \exp(i\Omega t)$ and $s_i^\pm \rightarrow s_i^\pm \exp(-i\Omega t)$ [2]. From the EOM, the frequency Ω of the rotating frame

is given by,

$$\Omega = \omega - 1 - \frac{1}{2} \sqrt{\frac{\kappa}{f_c}} \sqrt{2\lambda^2 - \kappa f_c}, \quad (3)$$

which eliminates the time evolution of $\phi + \psi$, so that it acquires a fixed arbitrary value. As a consequence of this U(1) symmetry (arbitrary $\phi + \psi$), the SR phase forms a continuous FPs lying on a circle in x - p and s_x - s_y plane with corresponding radius $\sqrt{2n^*}$ and $\sqrt{1 - s_z^{*2}}$ respectively.

The SR phase becomes unstable above a certain coupling strength $\lambda_I(\kappa)$, and the system exhibits oscillatory dynamics (see Fig.1(b)), which can be diagnosed by a single frequency peak in the fast Fourier transform (FFT) of $n_i(t), s_{zi}(t)$, as shown in the inset of Fig.1(b). With increasing λ , an intermediate regime emerges, where the dynamics exhibits oscillatory or chaotic behavior depending on the initial condition. The FFT of the chaotic trajectory shows the spreading of frequencies, whereas, for oscillatory dynamics, the FFT exhibits a single frequency. Further increasing the coupling strength, a chaotic phase is identified, as shown in the phase diagram, given in Fig.1(a) of the main text, where trajectories display a broadened power spectrum, as depicted in the inset of Fig.1(c). Chaotic dynamics can also be detected using the Lyapunov exponent (LE), which measures the sensitivity of the initial condition. Typically, for a chaotic trajectory, a small initial perturbation $\delta\mathbf{X}(t=0)$ at the phase space point \mathbf{X} grows exponentially in time $\|\delta\mathbf{X}(t)\| = e^{\Lambda t} \|\delta\mathbf{X}(0)\|$, which yields the Lyapunov exponent [1] as,

$$\Lambda = \lim_{t \rightarrow \infty} \frac{1}{t} \ln \left(\frac{\|\delta\mathbf{X}(t)\|}{\|\delta\mathbf{X}(0)\|} \right). \quad (4)$$

We compute the mean Lyapunov exponent (LE) $\bar{\Lambda}$, averaged over an ensemble of initial phase space points to quantify the degree of chaoticity, as shown in Fig.1(a) of the main text. In the oscillatory phase (OP), the LE is vanishingly small, on the contrary, chaotic regime is identified by large LE, as evident from Fig.1(a) of the main text.

To analyze the state of the system in the dynamically unstable regime with no stable FPs, we perform the truncated Wigner approximation (TWA), where the initial phase space points are sampled from a Gaussian distribution to mimic the quantum fluctuation. Each initial states are evolved separately up to a sufficiently long time and finally, we obtain the ensemble average of any observable as $\langle O \rangle_{\text{TWA}} = \sum_j O_j(t)/N$, where N is the number of trajectories with index j . Both in the oscillator and chaotic regime, even though the observables $O_j(t)$ along the individual classical trajectories exhibit time-dependent (irregular) oscillations, their ensemble at long time attains a stationary distribution (see Fig.1(e,f)), with time-independent ensemble average $\langle O \rangle_{\text{TWA}}$. The appearance of such stationary distribution of the observables describes the emergence of a steady state in the dynamically unstable regime, which smoothly connects to the stable SR phase. The evolution of the photon distribution in three different dynamical regimes is shown in Fig.1(d-f), which clearly manifests the delta-like distribution at n^* in the SR phase as it corresponds to the stable fixed point.

QUANTUM ERGODICITY AND STEADY STATE PROPERTIES

Here, we consider the nonequilibrium dynamics of the open TCD, particularly emphasizing the properties of the individual quantum trajectories, within the stochastic wavefunction approach. To investigate the ergodic property, we consider the time evolution of the observables along a typical quantum trajectory and obtain the time average of the observables such as $\langle \hat{n}_i \rangle_t$ and $\langle \hat{S}_{zi} \rangle_t$ up to sufficiently long time. Quantum mechanically, the ensemble average of the observables are described by their steady-state values $\langle \hat{n}_i \rangle_{\text{ss}}$ and $\langle \hat{S}_{zi} \rangle_{\text{ss}}$ (independent of the initial conditions), obtained from the steady state density matrix $\hat{\rho}_{\text{ss}}$. As evident from Fig.2(a,b), $\langle \hat{n}_i \rangle_t$ and $\langle \hat{S}_{zi} \rangle_t$ approach to $\langle \hat{n}_i \rangle_{\text{ss}}$ and $\langle \hat{S}_{zi} \rangle_{\text{ss}}$ respectively, clearly manifesting the ergodic nature of the steady state. Similar to the semiclassical analysis, the steady state remains ergodic across all dynamical phases over the large range of coupling strength λ . Additionally, in the chaotic regime, the Fourier spectrum of a typical quantum trajectory spreads over a range of frequencies, as depicted in Fig.2(c), indicating a signature of chaos [3].

To diagnose chaotic mixing, we study the nonequilibrium dynamics, starting from an arbitrary pure state, and obtain the evolution of entanglement entropy (EE) corresponding to one of the cavities. Both the growth rate and saturation value of EE increase in approach to the chaotic regime with increasing λ (see Fig.2(d)).

To understand the state of the photon field in the steady state of different regimes, we compute the Husimi distribution $Q(\alpha, \alpha^*) = \frac{1}{\pi} \langle \alpha | \hat{\rho}_{\text{Ph}} | \alpha \rangle$ from the reduced density matrix $\hat{\rho}_{\text{Ph}}$ of the photon field in one of the cavities, describing the semiclassical phase space density in $x - p$ plane. In the stable SR phase, the Husimi distribution forms a ring-like structure, peaked near the circle of classical fixed points with a radius $\sqrt{2n^*}$ and its spreading occurs as

a result of quantum fluctuations (see Fig.2(e)). In contrast, the semiclassical phase space density of photons in the chaotic regime is peaked at the center with an extended tail, resembling the thermal distribution, as shown in Fig.2(f).

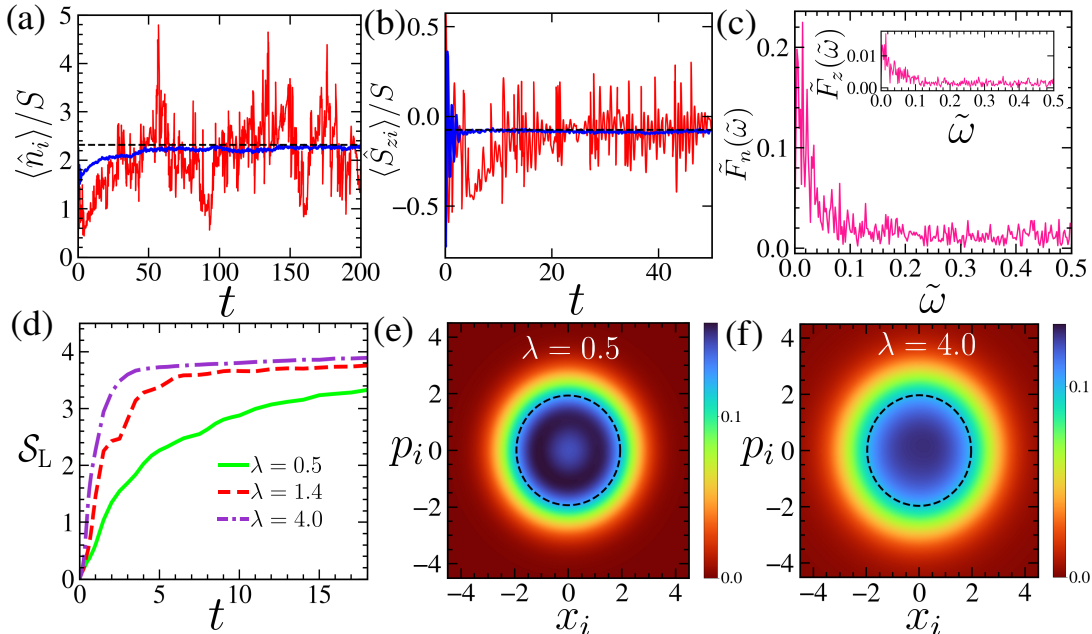


FIG. 2. *Quantum ergodicity*: Time evolution of (a) photon number $\langle \hat{n}_i \rangle$ and (b) spin polarization $\langle \hat{S}_{zi} \rangle$ of one of the cavities along single quantum trajectory (red) and their ensemble average (blue) in the chaotic regime. Black dashed lines are time average value of the single trajectory. (c) Fourier spectrum of $\langle \hat{n}_i \rangle$ (inset corresponds to $\langle \hat{S}_{zi} \rangle$) along single quantum trajectory. (d) The evolution of entanglement entropy \mathcal{S}_L of the left cavity for different λ . The Husimi distribution of the photon field in $x-p$ plane of one cavity in the (e) stable SR phase ($\lambda = 0.5$) and (f) chaotic phase ($\lambda = 4.0$). The black dashed circles in (e, f) represent the FPs of stable and unstable SR phase respectively. Panels (a-c) correspond to $\lambda = 4.0$. We set $\hbar, k_B = 1$ and $\omega = 2.0, \omega_0 = 0.5, \kappa = 0.05, \gamma_\uparrow = 0.2, \gamma_\downarrow = 0.1, S = 2$ for all figures.

SUBSYSTEM THERMALIZATION

As discussed in the main text, the reduced density matrix (DM) of subsystem A , $\hat{\rho}_A^{\text{ss}}$ corresponding to the steady state can be well described by the reduced DM $\hat{\rho}_A^{\text{th}}$ obtained from the thermal state of the isolated TCD within generalized Gibb's ensemble. We compute the trace-distance (TD) $\mathcal{T}_A = \text{Tr} \sqrt{(\hat{\rho}_A^{\text{ss}} - \hat{\rho}_A^{\text{th}})^\dagger (\hat{\rho}_A^{\text{ss}} - \hat{\rho}_A^{\text{th}})}$ between $\hat{\rho}_A^{\text{ss}}$ and thermal DM $\hat{\rho}_A^{\text{th}}$ to quantify their difference. As evident from Fig.3(a), the TD remains small compared to unity over a large range of λ , indicating the similarity between $\hat{\rho}_A^{\text{ss}}$ and $\hat{\rho}_A^{\text{th}}$, ensuring the validity of subsystem thermalization. Consequently, the average of local observables, such as the steady state value of the photon number $\langle \hat{n}_i \rangle_{\text{ss}}$ and spin polarization $\langle \hat{S}_{zi} \rangle_{\text{ss}}$ are in good agreement with the corresponding values obtained from the thermal state $\hat{\rho}^{\text{th}}$ (see Fig.3(b)). In the chaotic regime, a comparison of the angular averaged Husimi distribution $\bar{Q}(r) = \int_0^{2\pi} Q(r, \theta) d\theta$ between the photon field of steady state and thermal state is presented in Fig.3(c).

STATISTICS OF LIOUVILLIAN SPECTRUM

We analyze the spectrum of the Liouvillian superoperator

$$\hat{\mathcal{L}} = -i[\hat{\mathcal{H}} \otimes \mathbb{I} - \mathbb{I} \otimes \hat{\mathcal{H}}] + \kappa \sum_i \mathcal{D}[\hat{a}_i] + \frac{1}{S} \sum_i (\gamma_\uparrow \mathcal{D}[\hat{S}_{i+}] + \gamma_\downarrow \mathcal{D}[\hat{S}_{i-}]), \quad (5)$$

with $\mathcal{D}[\hat{L}] = \frac{1}{2} (2\hat{L} \otimes \hat{L}^* - \hat{L}^\dagger \hat{L} \otimes \mathbb{I} - \mathbb{I} \otimes \hat{L}^{\text{TR}} \hat{L}^*)$, where the superscript TR denotes the transposition. We construct the Liouvillian $\hat{\mathcal{L}}$ given above in the chaotic regime, considering spin $S = 2$ and bosonic number state up to $N_{\text{cutoff}} = 5$.

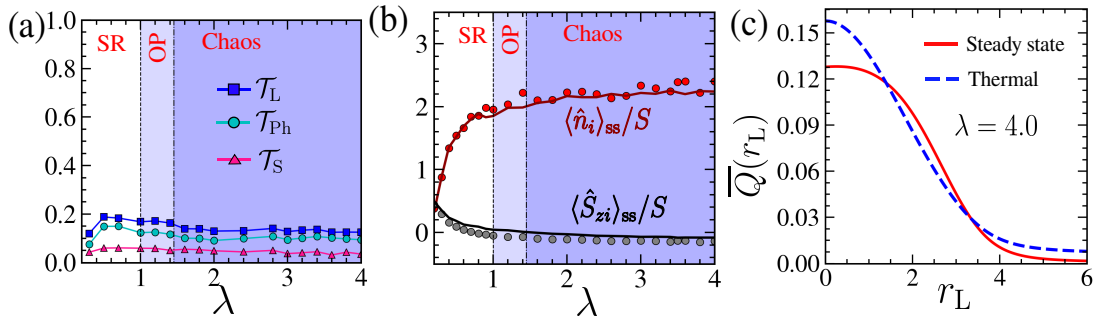


FIG. 3. Variation of (a) trace-distance \mathcal{T}_A between the reduced DM of steady state $\hat{\rho}_A^{\text{ss}}$ and thermal state $\hat{\rho}_A^{\text{th}}$ corresponding to the left cavity (\mathcal{T}_L), photon field (\mathcal{T}_{Ph}) and spin (\mathcal{T}_S) with λ . (b) The photon number $\langle \hat{n}_i \rangle_{\text{ss}}$ and spin polarization $\langle \hat{S}_{zi} \rangle_{\text{ss}}$ corresponding to the steady state (solid line) and thermal state (circles), as a function of λ . (c) Comparison of angular averaged Husimi $\bar{Q}(r_L)$ between the steady state (solid line) and thermal state (dashed line) in the chaotic regime ($\lambda = 4.0$).

The complex eigenvalues E_ν of the Liouvillian can be obtained from diagonalization of the non-hermitian matrix $\hat{\mathcal{L}}$. The pattern of the eigenvalues in the complex plane is shown in Fig.4(a), which is symmetric about the negative real axis. Next, we compute the complex spacing ratio (CSR) [4],

$$\xi_\nu = \frac{E_\nu^{\text{NN}} - E_\nu}{E_\nu^{\text{NNN}} - E_\nu}, \quad (6)$$

where E_ν^{NN} and E_ν^{NNN} are the nearest and next-nearest neighbours of the complex eigenvalue E_ν , which is a generalization of the adjacent gap ratio in the Hamiltonian system. It is evident from Fig.4(b), that the distribution of CSR is uniform in the complex plane, which is a universal feature of independent complex numbers, following 2d-Poisson statistics of random matrix theory (RMT) [4]. To quantify such universality in a spectrum, we compute $\langle r \rangle$ and $\langle \cos \theta \rangle$, where r_ν and θ_ν are the absolute value and argument of ξ_ν respectively, which agrees well with that of 2d-Poisson distribution with $\langle r \rangle \approx 0.67$ and $\langle \cos \theta \rangle = 0$. The corresponding level spacing (Euclidean distance δ between the nearest neighbours) distribution also agrees with the 2d-Poisson distribution, given by $P_{2\text{d-P}}(\delta) = \frac{\pi}{2} \delta \exp(-\pi \delta^2/4)$ [4], as depicted in Fig.4(c). On the other hand, the presence of level repulsion in the spectrum is manifested by the level spacing distribution following the GinUE statistics of RMT with $P(\delta) \sim \delta^3$ for small δ . The corresponding CSR exhibits $\langle r \rangle \approx 0.74$ and $\langle \cos \theta \rangle = -0.24$ [4]. However, in the present case, we do not find any signature of level repulsion in the Liouvillian spectrum corresponding to the classical chaotic regime.

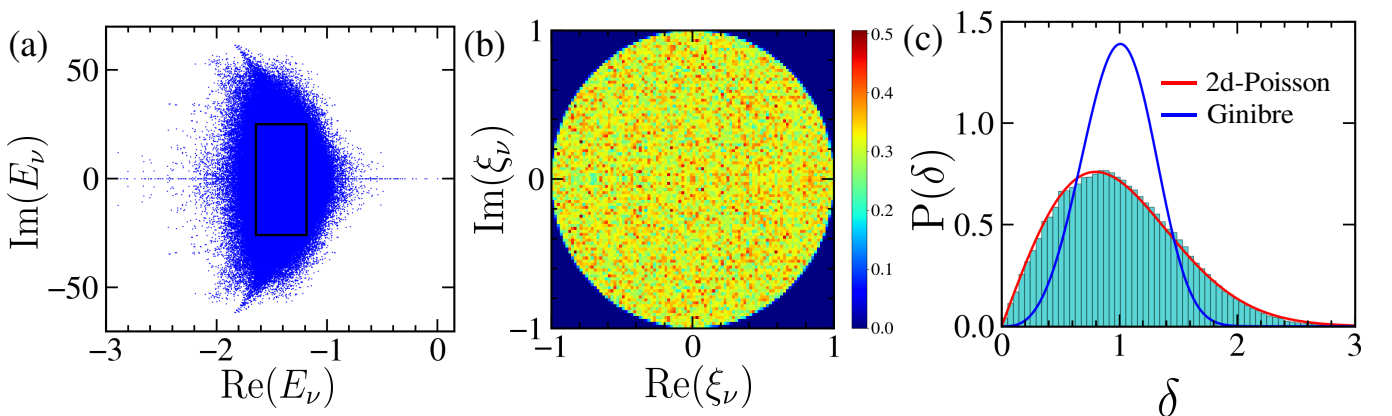


FIG. 4. Statistics of the Liouvillian spectrum in the classically chaotic regime: (a) The eigenvalues of the Liouvillian in the complex plane. (b) The distribution of the CSR ξ_ν in complex plane as color scale. (c) The level spacing distribution $P(\delta)$. We consider the eigenvalues within the black square in (a) for statistics. Parameter chosen: $\lambda = 4.0, \kappa = 0.05, \gamma_\downarrow = 0.1, \gamma_\uparrow = 0.2$.

-
- [1] S. H. Strogatz, *Nonlinear Dynamics and Chaos* (Westview Press, Boulder, CO, 2007).
 - [2] W. Kopylov, M. Radonjić, T. Brandes, A. Balaž, and A. Pelster, *Phys. Rev. A* **92**, 063832 (2015).
 - [3] T. Geisel, *Phys. Rev. A* **41**, 2989 (1990); Erratum *Phys. Rev. A* **42**, 7491 (1990).
 - [4] L. Sá, P. Ribeiro, and T. Prosen, *Phys. Rev. X* **10**, 021019 (2020).